Realizing double Dirac particles in the presence of electronic interactions

Domenico Di Sante,[1] Andreas Hausoel,[1] Paolo Barone,[2] Jan M. Tomczak,[3] Giorgio Sangiovanni,[1] and Ronny Thomale[1]

[1]*Institut für Theoretische Physik und Astrophysik, Universität Würzburg, Am Hubland Campus Süd, Würzburg 97074, Germany*
[2]*Consiglio Nazionale delle Ricerche (CNR-SPIN), Via Vetoio, L'Aquila, Italy*
[3]*Institute of Solid State Physics, Vienna University of Technology, A-1040 Vienna, Austria*

Double Dirac fermions have recently been identified as possible quasiparticles hosted by three-dimensional crystals with particular nonsymmorphic point-group symmetries. Applying a combined approach of *ab initio* methods and dynamical mean-field theory, we investigate how interactions and double Dirac band topology conspire to form the electronic quantum state of Bi_2CuO_4. We derive a downfolded eight-band model of the pristine material at low energies around the Fermi level. By tuning the model parameters from the free band structure to the realistic strongly correlated regime, we find a persistence of the double Dirac dispersion until its constituting time-reversal symmetry is broken due to the onset of magnetic ordering at the Mott transition. Our calculations suggest that the double Dirac fermions in Bi_2CuO_4 can be restored by experimentally accessible hydrostatic pressures. In light of the growing attention to the topological quantum chemistry approach, our results on Bi_2CuO_4 show how many-body effects must be included beyond the static mean-field level for reliable predictions on new materials.

Introduction. Electrons in solids witness a reduced spatial symmetry in comparison to the space-time continuum. While the high-energy perspective constrains us to Majorana, Weyl, and Dirac fermions in accordance with the inhomogeneous Lorentz (or Poincaré) group, electronic quasiparticles in solids at low energies can display emergent fermionic behavior within and even beyond this classification [1,2]. Graphene constitutes one of the most prominent material discoveries where Dirac-type quasiparticles have been realized [3]. The current rise of Weyl semimetals [4], along with Majorana quasiparticles in superconducting heterostructures [5,6], complements this evolution in contemporary condensed-matter physics.

Recently, Wieder *et al.* [1] have brought up the possibility to realize double Dirac quasiparticles in certain three-dimensional (3D) crystals with specific nonsymmorphic point-group symmetry. Such type of fermion does not exist in high-energy physics due to its incompatibility with the Lorentz group, and highlights the relevance of lattice fermion realizations not only in terms of quantum many-body, but also single-particle states of matter. Double Dirac fermions were identified by a systematic analysis of all double space groups (SGs) accounting for $S = 1/2$ electrons in spin-orbit coupled crystals with time-reversal symmetry [2]. In particular, SG 130 and 135 were found to establish eminently suited ground for generic double Dirac fermions protected by point-group symmetry. Among all material candidates for SG 130, it was already realized in Ref. [2] that Bi_2CuO_4 might be a prime candidate due to its filling-enforced semimetallicity [7], nurturing the hope to observe double Dirac fermions close to the Fermi level. All such band-structure classifications, however, always need to be extended to account for the role of interactions in the material, which turn out to be of vital relevance in Bi_2CuO_4. Most of the topological band properties, even the metallic ones, display a certain degree of persistence against weak interactions as long as those do not break any protecting symmetry. Interaction-induced instabilities,

however, do change the symmetry class of the quantum state, possibly affecting the whole range of constituting symmetries including charge conservation, time-reversal, and point-group operations.

As a paradigmatic change, the concept of topological quantum chemistry is firmly emerging, based on the idea that quantum chemistry and topology conspire to provide a new search principle for topological quantum states of matter [8]. Many new topological insulator and semimetal candidates were revealed within such a framework, where, however, strong electron interactions are neglected. In this Rapid Communication, to show how crucial it is for this search to go beyond the single-particle description, we study strong interaction effects of double Dirac fermions, analyzing the band-structure properties and electronic correlations in Bi_2CuO_4. From density functional theory, we distill an effective eight-band tight-binding Hubbard model which is dominated by the $d_{x^2-y^2}$ orbital of the four Cu atoms in the unit cell. Spin-orbit coupling (SOC) is found to be weak because the heavy atoms of the compound do not significantly contribute to the low-energy density of states. As expected, the double Dirac dispersion is located close to the Fermi energy, as identified by an eightfold band degeneracy at the A point. We quantify the strength of electron-electron interactions by means of the constrained random phase approximation (cRPA). By employing a combined approach of density functional theory (DFT) and dynamical mean-field theory (DMFT), we determine the critical value for the Mott transition at ambient pressure to be $U_{Mott} \approx 0.85$ eV. This value is approximately equal to the $d_{x^2-y^2}$ bandwidth, and substantially smaller than $U_{cRPA} \approx 1.58$ eV [9], suggesting that Bi_2CuO_4 at ambient pressure parametrically locates itself deep in the Heisenberg limit of the Mott regime. Below the Néel temperature T_N, the magnetic state displays an antiferromagnet C-type (AFM-C) collinear order of the four local Cu magnetic moments. In the stochiometric compound at pristine conditions, magnetism thus dominates the electronic
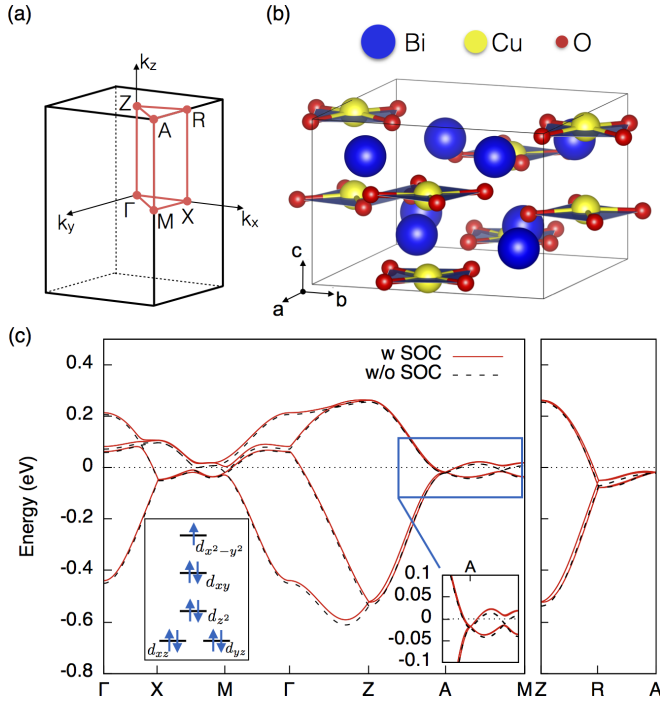
FIG. 1. (a) Tetragonal Brillouin zone of SG 130 $P4/ncc$ with corresponding high-symmetry points. (b) Crystal structure of Bi_2CuO_4. Atom colors: Bi (blue), Cu (yellow), and O (red). Blue plaquettes highlight the square-planar CuO_4 coordination. (c) DFT band structure in the paramagnetic metallic phase with (red solid line) and without (black dashed line) SOC. The left inset is a schematic representation of the square-planar crystal field and orbital filling for Cu-type d^9. The right inset shows a zoom around the eightfold degenerate A point, which comes along a characteristic fourfold degeneracy along the R-Z line.

state, rendering the double Dirac fermions inaccessible. We explore the effect of hydrostatic pressure to drive Bi_2CuO_4 into a metallic phase where the double Dirac fermions emerge. We find the band-structure formation and correlation effects of Bi_2CuO_4 to be highly sensitive to pressure. Starting from ambient pressure, we find an initial change of the magnetic ordering from AFM-C to AFM-G type, along with a reduced on-site Coulomb repulsion. This could pave the way toward a high-pressure double Dirac metal.

Band structure and effective tight-binding model. Bi_2CuO_4 crystallizes in the tetragonal space group $P4/ncc$ (SG 130) [Fig. 1(a)] [11]. Four inequivalent Cu in the unit cell share a square-planar CuO_4 coordination, stacked along the out-of-plane direction and intercalated by Bi atoms, as depicted in Fig. 1(b). The Cu-O hybridization is quite strong, leading to a mixed d-p character of the band structure of the occupied states [12]. The Bi-p manifold only starts ≈ 1.5 eV above the Fermi level, suggesting that the low-energy model is given by Cu and O electronic states. The square-planar crystal field is characterized by a higher-in-energy $d_{x^2-y^2}$ orbital experiencing a head-to-head interaction with the O-p. The level separation is schematically drawn in the left inset of Fig. 1(c). Cu is nominally in the oxidation state 2+ (i.e., d^9 configuration). For this reason, a half-filled $d_{x^2-y^2}$-derived single spin-degenerate band per Cu atom in the unit cell is
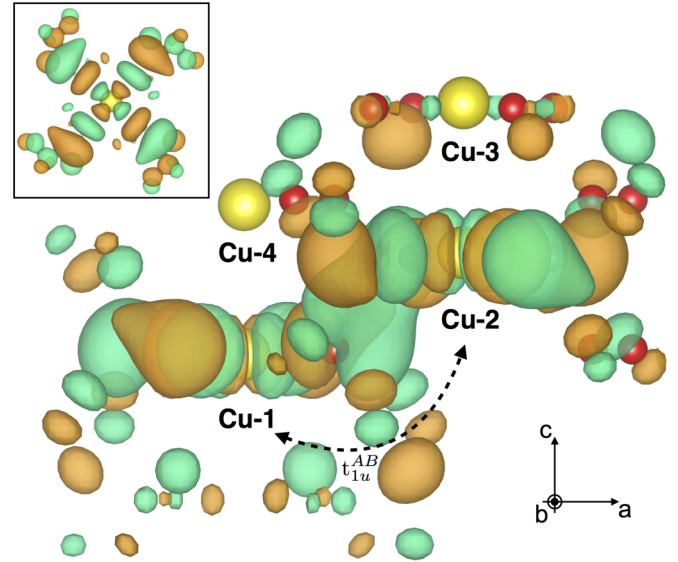
FIG. 2. Side view of the $d_{x^2-y^2}$-type MLWFs belonging to two neighboring Cu chains, responsible for the transfer integral t_{1u}^{AB} (Table I). Brown (green) color refers to positive (negative) values of the MLWF. The individual MLWFs are not symmetric with respect to the CuO_4 plaquette plane. This is due to a small off-centering of the Cu atoms, in opposite directions for Cu-1 and Cu-2. The inset shows a top view on the Cu-1 $d_{x^2-y^2}$-type MLWF.

expected to dominate at low energies. Figure 1(c) displays the band dispersion of the electronic states around the Fermi level. Due to the dominant Cu orbital, the effect of SOC is almost negligible, only inducing small spin splittings. We estimate the energy scale of SOC to be ≈ 20 meV. Despite its small scale, however, SOC is a crucial ingredient for the symmetries in the double SG representation that ensures the existence of a double Dirac fermion with linear dispersion at the Brillouin zone corner $A = (\pi,\pi,\pi)$. As the band filling is given by an odd multiple of 4 ($180 = 8 \times 22 + 4$), the double Dirac fermion in Bi_2CuO_4 is located almost at the Fermi level, as visible in the right inset of Fig. 1(c).

While the aforementioned electronic structure details, as well as the magnetic properties at ambient pressure, have already been analyzed previously [10,13], a closer inspection of the hybridization profile and the Coulomb matrix elements in terms of *ab initio* derived maximally localized Wannier functions (MLWFs) [14] is indispensable to further analyze the fate of double Dirac fermions in the presence of interactions. The relatively large extension of the MLWFs is a consequence of the strong Cu-O hybridization. Their lobes indeed stretch out over the O atoms with a clockwise winding shape, as shown in the top view of Fig. 2. Our analysis elucidates the origin of the strong three-dimensional character of Bi_2CuO_4, as the MLWFs extend along the out-of-plane direction in an asymmetric manner, which is a consequence of buckled CuO_4 plaquettes. Moreover, two $d_{x^2-y^2}$-type MLWFs localized on different chains have a strong overlap, even though they do not belong to the same ab plane. This is illustrated by the t_{1u}^{AB} transfer integral shown in Fig. 2 and Table I. Coherent electron hopping is also enabled between neighboring plaquettes along the normal c direction. This process is accounted for by the

TABLE I. Hopping integrals in meV between the $d_{x^2-y^2}$-type Wannier functions on different Cu atoms for different pressure P (GPa) with ambient pressure $P = 0$ GPa. The first row takes over the notation introduced in Ref. [10], while $t_{i,j}$ in the second row is the transfer integral between the Cu-i and Cu-j sites ($i, j = 1 \ldots 4$) as in Fig. 2. When a j index has a superscript ± 1 it refers to a Cu-j atom in the $[00 \pm 1]$ unit cell. U_{cRPA} (eV) is the cRPA value for the effective on-site Coulomb interaction [9]. The $P = 0$ hopping values in parentheses refer to Ref. [10].

P	t^{AB}_{1u} $t_{1,2}$	t^{AB}_{1d} $t_{4,2}$	t^{AB}_{2u} $t_{1,3}$	t^{AB}_{2d} $t_{1,2^{-1}}$	t^A_1 $t_{1,4}$	t^A_2 $t_{1,1^1}$	U_{cRPA}
0	66	40	5	-24	36	-20	1.58
	(74)	(36)	-	(-40)	(21)	(-18)	
30	80	21	6	-20	73	-16	1.45
50	88	13	2	-13	65	-7	1.36

transfer integral t^A_1, which is indeed comparable with the hoppings t^{AB}_{1u} and t^{AB}_{1d} that involve a significant in-plane component. As further discussed below, the hoppings turn out to be rather sensitive to pressure, and even impose a change of the magnetic ordering pattern, which is relevant to classifying the possible topological character of symmetry-broken phases in $\mathrm{Bi_2CuO_4}$ [15].

Mott transition and spectral function. Having obtained an effective band-structure description of $\mathrm{Bi_2CuO_4}$ close to E_F in terms of a half-filled single band per Cu atom, we focus on the double Dirac point at the A point. In particular, we analyze its evolution as a function of interaction strength, starting from the free-electron limit up to the realistic cRPA value for the electron-electron interaction U [9]. $\mathrm{Bi_2CuO_4}$ is parametrically located within the applicability bounds of DFT+DMFT, partly because of its three-dimensional character. Figure 3(a) displays the quasiparticle weight $Z = (1 - \partial \mathrm{Re}\Sigma(\omega)/\partial\omega|_{\omega \to 0})^{-1}$. Before reaching U_{cRPA}, we encounter a Mott-type metal-to-insulator transition at $U_{\mathrm{Mott}} \approx 0.85$ eV. At the Mott transition, the quasiparticle weight is suppressed by interactions, and the

fraction of doubly occupied Cu sites $\langle n_\uparrow n_\downarrow \rangle$ reduces from the free-particle value of $1/4$ toward zero [inset in Fig. 3(a)]. At intermediate U, the spectral function, as depicted in Fig. 3(b), is well described by the DFT single-particle band structure renormalized in terms of bandwidth by the quasiparticle weight Z, along with the appearance of incoherent lower and upper Hubbard bands. Since the double Dirac fermion is located close to the Fermi level, it contributes to the quasiparticle peak for interaction strengths below the Mott transition. Even though the eightfold degeneracy at the A point remains discernible up to U_{Mott}, the Coulomb repulsion has a dramatic effect on the double Dirac feature. The velocities are substantially reduced and the linewidths increase rapidly due to the strong scattering. Even if the protecting symmetry is not yet broken by the magnetic ordering, the damping of the band structure as well as the transfer of spectral weight toward high-energy (Hubbard) bands are so pronounced that the whole double Dirac feature loses most of its distinctness already for $U \ll U_{\mathrm{Mott}}$.

Magnetic order and hydrostatic pressure. At U_{cRPA}, allowing for magnetic ordering, the ground state of $\mathrm{Bi_2CuO_4}$ is not paramagnetic, but displays intra-unit-cell magnetic order. As a consequence, the Mott regime and the breaking of time-reversal symmetry independently suggest the absence of double Dirac cones. In Table II, we report the DFT+U energies at $T = 0$ for different magnetic configurations. Mapping these energies on a Heisenberg model and performing classical Monte Carlo simulations, we estimate a Néel temperature of 56 K for $U = 1.58$ eV, which compares reasonably well with the experimental value of 50 K [10–12]. The AFM-C type configuration, characterized by a ferromagnetic alignment of the chains along the c direction, is found to be preferred. Independent of the considered interaction strength, however, it is always energetically close to an AFM-G type phase, where the magnetic moments are antiferromagnetically aligned along all three directions. This is the consequence of a competitive balance between t^A_1 and t^{AB}_{1d} transfer integrals (Table I). This tuned frustration is relieved by pressure, favoring t^A_1 over t^{AB}_{1d}.
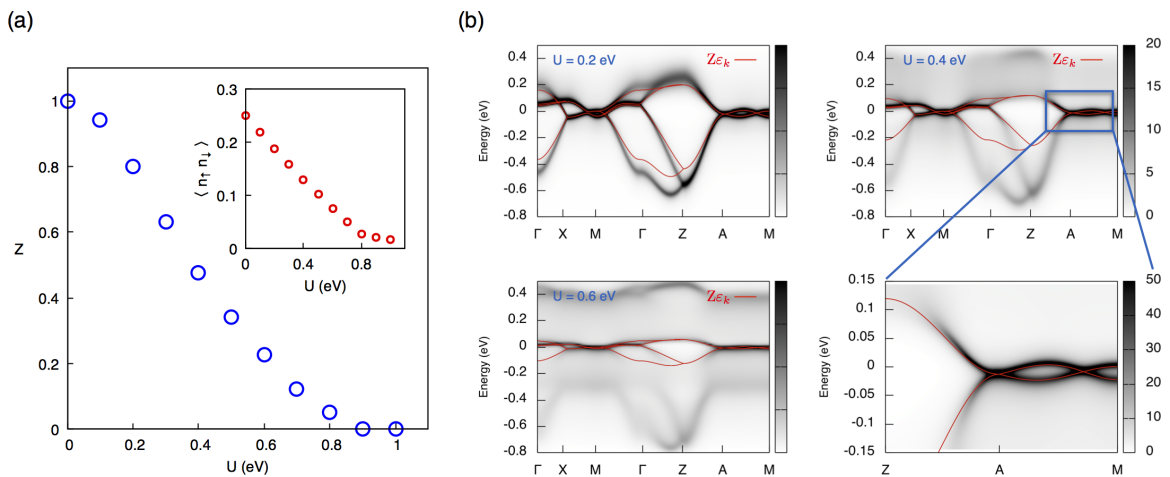
FIG. 3. (a) DMFT quasiparticle weight Z (main panel) and double occupancies (inset) as a function of U in the paramagnetic phase for a temperature $\beta = 100$ eV^{-1}. The Mott transition occurs at $U_{\mathrm{Mott}} \approx 0.85$ eV. (b) Momentum-resolved DMFT spectral function $A(k,\omega)$ for $U = 0.2, 0.4,$ and 0.6 eV. Red lines denote the DFT band structure renormalized by the DMFT quasiparticle weight Z. For $U = 0.4$ eV, the zoom shows the preservation of the eightfold degenerate A point along with an already significant band renormalization.

TABLE II. DFT+U total energy differences (meV/unit cell) for the magnetic patterns at ambient pressure and at 30 GPa. The lowest-lying AFM-type state is chosen as reference energy. Nonmagnetic (NM) and ferromagnetic (FM) configurations are higher up in energy than the AFM states.

P (GPa)	U (eV)	NM	FM	AFM-C	AFM-G	AFM-A
0						
	0.0	442	88	0	2.4	54
	0.5	555	77	0	2.2	49
	1.58	812	60	0	1.8	41
	2.1	940	54	0	1.6	37
30						
	1.45	636	97	28	0	65

It explains why we observe a change to AFM-G type magnetic order as a function of pressure (see Table II).

Along with the change of the magnetic order, pressure has a profound impact on the electronic structure. As illustrated in Figs. 4(a)–4(c), the bands above and below the $d_{x^2-y^2}$ manifold get closer to the Fermi level. This results in a more efficient screening of the Coulomb interaction for the target $d_{x^2-y^2}$ states. Figure 4(d) and Table I report the corresponding reduction of U_{cRPA}. In addition, the slight increase of the $d_{x^2-y^2}$ bandwidth (~10%) leads to a larger critical U_{Mott} for the Mott

FIG. 4. (a)–(c) Evolution of the DFT band structure for $P = 0$ (ambient pressure), 6, and 30 GPa. Red symbols refer to the $d_{x^2-y^2}$ character. (d) U_{cRPA} and U_{Mott} as a function of pressure. It is suggestive to expect an insulator to metal transition around $P = 50$–60 GPa. (e),(f) Momentum-resolved DMFT spectral function $A(k,\omega)$ for $U = 0.85$ and 0.95 eV at a pressure $P = 50$ GPa. A two-color palette has been used to better highlight the linear dispersion along the Z-A line. The maximum color intensity (arb. units) in panel (e) is twice as large as that in panel (f).

transition. Even though U_{cRPA} remains larger than U_{Mott} all the way up to 50 GPa [16], the trend toward the restoration of the metallic phase is evident [17], as shown in Figs. 4(d)–4(f). Assuming the absence of a structural phase transition [16], this suggests a transition into a high-pressure double Dirac metal for $\simeq 60$ GPa.

Conclusion. Our analysis identifies Bi_2CuO_4 as a prototypical material where crystal structure and orbital character, under pressure, conspire to give rise to correlated double Dirac fermions close to the Fermi level. At ambient pressure, the interactions turn out to drive the system into a Mott state along with magnetic intracell ordering where the double Dirac cone is absent. As a function of hydrostatic pressure, we find that the material could be driven into a metallic state where the double Dirac features would emerge. For this, our *abinitio* calculations indicate a pressure regime of ≈ 60 GPa, which is still within the range of experimental pressure cell transport setups. Our study suggests several routes to realize a double Dirac metal in Bi_2CuO_4 at low temperatures. For instance, a combined pressure and doping approach could establish a convenient perturbation of the pristine material in order to render correlated double Dirac fermions accessible to experimental investigation.

Besides the specific example of double Dirac fermions in Bi_2CuO_4, in this Rapid Communication we comunicate a rather general message, namely, that all these new topological quantum chemistry developments need to be looked at more carefully, as interactions are systematically neglected [8]. This may constitute the most severe and harsh drawback of the whole approach, largely based on the single-particle band theory of electrons. On the other hand, we demonstrated how it is possible to restore the nontrivial new quasiparticle physics by means of external handles, in this way curing the intrinsic failure of the topological quantum chemistry machinery.

This is crucial in light of future technological applications of such new quasiparticles. To give an example, it will be of relevant interest to study the effects of a magnetic field imposed on the double Dirac particle dispersion, similarly to what has been done in the case of Dirac and Weyl semimetals [18,19]. Centered in the same conal center, the double Dirac particle features two Dirac cones of different opening angles. As a function of these angles, it is reasonable to foresee an unprecedented variety of band decompositions that promises to happen in response to a magnetic field, along with a likely highly nontrivial magnetoresistance profile. However, in analogy to the Fermi velocity renormalization effect by interactions in graphene [20], the renormalization of the double Dirac cone dispersion will play a quantitative key role.

[1] B. J. Wieder, Y. Kim, A. M. Rappe, and C. L. Kane, Phys. Rev. Lett. **116**, 186402 (2016).

[2] B. Bradlyn, J. Cano, Z. Wang, M. G. Vergniory, C. Felser, R. J. Cava, and B. A. Bernevig, Science **353**, aaf5037 (2016).

[3] A. H. Castro Neto, F. Guinea, N. M. R. Peres, K. S. Novoselov, and A. K. Geim, Rev. Mod. Phys. **81**, 109 (2009).

[4] X. Wan, A. M. Turner, A. Vishwanath, and S. Y. Savrasov, Phys. Rev. B **83**, 205101 (2011).

[5] N. Read and D. Green, Phys. Rev. B **61**, 10267 (2000).

[6] L. Fu and C. L. Kane, Phys. Rev. Lett. **100**, 096407 (2008).

[7] H. C. Po, H. Watanabe, M. P. Zaletel, and A. Vishwanath, Sci. Adv. **2**, e1501782 (2016).

[8] B. Bradlyn, L. Elcoro, J. Cano, M. G. Vergniory, Z. Wang, C. Felser, M. I. Aroyo, and B. A. Bernevig, Nature (London) **547**, 298 (2017).

[9] Here, we define the value for U_{cRPA} as the local minus the nearest-neighbor part of the cRPA Coulomb matrix element.

[10] O. Janson, R. O. Kuzian, S.-L. Drechsler, and H. Rosner, Phys. Rev. B **76**, 115119 (2007).

[11] J. L. Garcia-Munoz, J. Rodriguez-Carvajal, F. Sapina, M. J. Sanchis, R. Ibanez, and D. Beltran-Porter, J. Phys.: Condens. Matter **2**, 2205 (1990).

[12] See Supplemental Material at http://link.aps.org/supplemental/10.1103/PhysRevB.96.121106 for more computational details, including cRPA and GW calculations. The Supplemental Material includes Refs. [21–42].

[13] A. Goldoni, U. del Pennino, F. Parmigiani, L. Sangaletti, and A. Revcolevschi, Phys. Rev. B **50**, 10435 (1994).

[14] N. Marzari, A. A. Mostofi, J. R. Yates, I. Souza, and D. Vanderbilt, Rev. Mod. Phys. **84**, 1419 (2012).

[15] A. Schnyder (private communication).

[16] So far, pressure effects have been hardly investigated in Bi_2CuO_4. In [43], the occurrence of a structural phase transition might have been observed within 20 and 37 GPa, but demands further analysis.

[17] The most reliable feature is the trend observed as a function of pressure rather than the absolute values of the Coulomb interaction strength obtained through cRPA. The absolute accuracy of cRPA is challenged by (i) the slight tendency to underestimate the Coulomb matrix elements, (ii) the mapping of the nonlocal cRPA Coulomb interaction onto a local Hubbard model, and (iii) the absence of all nonlocal correlations within the DMFT approximation. The latter is known to reduce the Néel temperature of about 30%–40% in 3D systems [44].

[18] A. C. Potter, I. Kimchi, and A. Vishwanath, Nat. Commun. **5**, 5161 (2014).

[19] J. Klier, I. V. Gornyi, and A. D. Mirlin, Phys. Rev. B **92**, 205113 (2015).

[20] D. C. Elias, R. V. Gorbachev, A. S. Mayorov, S. V. Morozov, A. A. Zhukov, P. Blake, L. A. Ponomarenko, I. V. Grigorieva, K. S. Novoselov, F. Guinea, and A. K. Geim, Nat. Phys. **7**, 701 (2011).

[21] G. Kresse and J. Furthmüller, Phys. Rev. B **54**, 11169 (1996).

[22] P. E. Blöchl, Phys. Rev. B **50**, 17953 (1994).

[23] G. Kresse and D. Joubert, Phys. Rev. B **59**, 1758 (1999).

[24] J. P. Perdew, K. Burke, and M. Ernzerhof, Phys. Rev. Lett. **77**, 3865 (1996).

[25] S. Steiner, S. Khmelevskyi, M. Marsmann, and G. Kresse, Phys. Rev. B **93**, 224425 (2016).

[26] A. A. Mostofi, J. R. Yates, Y.-S. Lee, I. Souza, D. Vanderbilt, and N. Marzari, Comput. Phys. Commun. **178**, 685 (2008).

[27] A. Georges, G. Kotliar, W. Krauth, and M. J. Rozenberg, Rev. Mod. Phys. **68**, 13 (1996).

[28] E. Gull, A. J. Millis, A. I. Lichtenstein, A. N. Rubtsov, M. Troyer, and P. Werner, Rev. Mod. Phys. **83**, 349 (2011).

[29] N. Parragh, A. Toschi, K. Held, and G. Sangiovanni, Phys. Rev. B **86**, 155158 (2012).

[30] F. Aryasetiawan, M. Imada, A. Georges, G. Kotliar, S. Biermann, and A. I. Lichtenstein, Phys. Rev. B **70**, 195104 (2004).

[31] T. Miyake and F. Aryasetiawan, Phys. Rev. B **77**, 085122 (2008).

[32] M. Methfessel, M. van Schilfgaarde, and R. Casali, in *Electronic Structure and Physical Properties of Solids: The Uses of the LMTO Method*, edited by H. Dreysse, Lecture Notes in Physics Vol. 535 (Springer-Verlag, Berlin, 2000), p. 114.

[33] S. V. Faleev, M. van Schilfgaarde, and T. Kotani, Phys. Rev. Lett. **93**, 126406 (2004).

[34] J. M. Tomczak, J. Phys.: Conf. Ser. **592**, 012055 (2015).

[35] P. Seth, P. Hansmann, A. van Roekeghem, L. Vaugier, and S. Biermann, Phys. Rev. Lett. **119**, 056401 (2017).

[36] A. Abdulkarem, J. Li, A. Aref, L. Ren, E. Elssfah, H. Wang, Y. Ge, and Y. Yu, Mater. Res. Bull. **46**, 1443 (2011).

[37] N. T. Hahn, V. C. Holmberg, B. A. Korgel, and C. B. Mullins, J. Phys. Chem. C **116**, 6459 (2012).

[38] T. Arai, M. Yanagida, Y. Konishi, Y. Iwasaki, H. Sugihara, and K. Sayama, J. Phys. Chem. C **111**, 7574 (2007).

[39] J. M. Tomczak, M. van Schilfgaarde, and G. Kotliar, Phys. Rev. Lett. **109**, 237010 (2012).

[40] J. M. Tomczak, T. Miyake, and F. Aryasetiawan, Phys. Rev. B **81**, 115116 (2010).

[41] J. M. Tomczak, T. Miyake, R. Sakuma, and F. Aryasetiawan, Phys. Rev. B **79**, 235133 (2009).

[42] T. Schäfer, A. Toschi, and J. M. Tomczak, Phys. Rev. B **91**, 121107(R) (2015).

[43] F. X. Zhang, B. Manoun, S. K. Saxena, and C. S. Zha, J. Solid State Chem. **179**, 1202 (2006).

[44] G. Rohringer, A. Toschi, A. Katanin, and K. Held, Phys. Rev. Lett. **107**, 256402 (2011).